

$\gamma\delta$ TDEs: An Efficient Delivery System for miR-138 with Anti-tumoral and Immunostimulatory Roles on Oral Squamous Cell Carcinoma

Ling Li,^{1,6} Shun Lu,^{2,6} Xinhua Liang,³ Bangrong Cao,⁴ Shaoxin Wang,¹ Jian Jiang,¹ Huaichao Luo,⁵ Shuya He,⁵ Jinyi Lang,² and Guiquan Zhu¹

¹Department of Head and Neck Surgery, Sichuan Cancer Hospital & Institute, Sichuan Cancer Center, School of Medicine, University of Electronic Science and Technology of China, Chengdu, Sichuan 610041, P.R. China; ²Department of Radiation Oncology, Sichuan Cancer Hospital & Institute, Sichuan Cancer Center, School of Medicine, University of Electronic Science and Technology of China, Chengdu, Sichuan 610041, P.R. China; ³State Key Laboratory of Oral Diseases, West China Hospital of Stomatology, Sichuan University, Chengdu, P.R. China; ⁴Department of Basic Research, Sichuan Cancer Hospital & Institute, Sichuan Cancer Center, School of Medicine, University of Electronic Science and Technology of China, Chengdu, Sichuan 610041, P.R. China; ⁵Department of Clinical Laboratory, Sichuan Cancer Hospital & Institute, Sichuan Cancer Center, School of Medicine, University of Electronic Science and Technology of China, Chengdu, Sichuan 610041, P.R. China

In this study, we sought to investigate the potential application of $\gamma\delta$ T cell-derived extracellular vesicles ($\gamma\delta$ TDEs) as drug delivery system (DDS) for miR-138 in the treatment of oral squamous cell carcinoma (OSCC). Our data showed that over-expression of miR-138 in $\gamma\delta$ T cells obtained miR-138-rich $\gamma\delta$ TDEs accompanying increased expansion and cytotoxicity of $\gamma\delta$ T cells. $\gamma\delta$ TDEs inherited the cytotoxic profile of $\gamma\delta$ T cells and could efficiently deliver miR-138 to OSCC cells, resulting in synergetic inhibition on OSCC both *in vitro* and *in vivo*. The pre-immunization by miR-138-rich $\gamma\delta$ TDEs inhibited the growth of OSCC tumors in immunocompetent C3H mice, but not in nude mice, suggesting an immunomodulatory role by miR-138-rich $\gamma\delta$ TDEs. $\gamma\delta$ TDEs and miR-138 additively increased the proliferation, interferon- γ (IFN- γ) production, and cytotoxicity of CD8⁺ T cells against OSCC cells. Only delivered by $\gamma\delta$ TDEs can miR-138 efficiently target programmed cell death 1 (PD-1) and CTLA-4 in CD8⁺ T cells. We conclude that $\gamma\delta$ TDEs delivering miR-138 could achieve synergetic therapeutic effects on OSCC, which is benefited from the individual direct anti-tumoral effects on OSCC and immunostimulatory effects on T cells by both $\gamma\delta$ TDEs and miR-138; $\gamma\delta$ TDEs could serve as an efficient DDS for microRNAs (miRNAs) in the treatment of cancer.

INTRODUCTION

Oral squamous cell carcinoma (OSCC), which includes epithelial neoplasms of the oral cavity and oropharynx, is a serious and growing problem in many parts of the world. The annual estimated incidence is approximately 275,000 worldwide.¹ Despite numerous advances in the diagnosis and treatment of oral cancer, the 5-year survival rates for cancers of the tongue, oral cavity, and oropharynx are only approximately 50%.¹ The 5-year survival rate of patients with advanced disease (stages III/IV) is approximately 20%.² Current treatment modalities for locally advanced diseases, such as surgery,

radiotherapy, and chemotherapy, cause significant dysfunctions and toxicities, which emphasizes the necessity for new treatment options.³

$\gamma\delta$ T cells represent a minor lymphocyte population that constitute 0.5%–16% of total CD3⁺ cells in the peripheral blood, while predominating in the intestine and skin.⁴ The majority of human $\gamma\delta$ T cells express T cell receptor (TCR) V γ 9 and V δ 2 chains that can be activated in a major histocompatibility complex (MHC)-independent manner.⁵ When expanded *in vitro*, $\gamma\delta$ T cells isolated from patients with melanoma, glioblastoma, neuroblastoma, breast, lung, ovarian, colon, and pancreatic cancer efficiently killed tumor cell lines and/or primary cancer samples.⁶ In addition, activated $\gamma\delta$ T cells display phenotypic characteristics of professional antigen-presenting cells (APCs) and induce CD4⁺ and CD8⁺ T cell proliferation and cytotoxicity.⁷ This direct cytotoxicity against cancer cells and antigen-presenting characteristics make $\gamma\delta$ T cells good candidates for effective tumor immunotherapy.⁸ However, clinical trials exploiting $\gamma\delta$ T cells in several cancer types have been conducted over the past decade, with a good safety profile but somewhat conflicting results in most solid tumors.⁹ Migration and homing properties are important aspects of $\gamma\delta$ T cell physiology to consider for cancer immunotherapy.⁶ Thus, developing novel strategies to improve the

Received 28 July 2018; accepted 16 November 2018;
<https://doi.org/10.1016/j.omtn.2018.11.009>.

⁶These authors contributed equally to this work.

Correspondence: Jinyi Lang, Department of Radiation Oncology, Sichuan Cancer Hospital & Institute, Sichuan Cancer Center, School of Medicine, University of Electronic Science and Technology of China, No. 55, Section 4, Renmin South Road, Chengdu, Sichuan 610041, P.R. China.

E-mail: langjy610@163.com

Correspondence: Guiquan Zhu, Department of Head and Neck Surgery, Sichuan Cancer Hospital & Institute, Sichuan Cancer Center, School of Medicine, University of Electronic Science and Technology of China, No. 55, Section 4, Renmin South Road, Chengdu, Sichuan 610041, P.R. China.

E-mail: zgq@sichuancancer.org



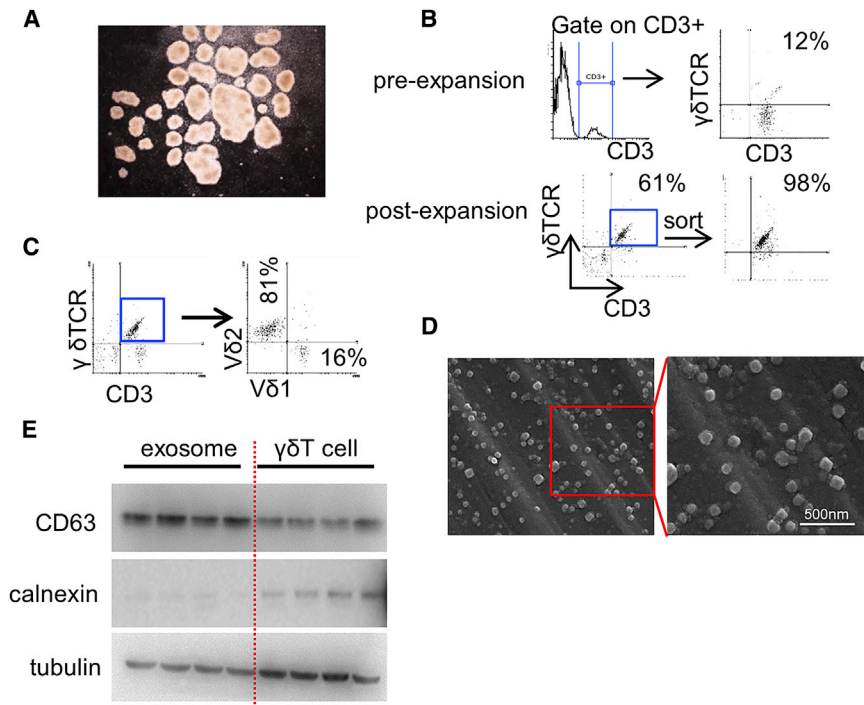


Figure 1. Expanded $\gamma\delta$ T Cells Produce Typical EVs

(A) Representative image of $\gamma\delta$ T cells cultured *in vitro*. (B) Representative flow cytometry of $\gamma\delta$ T cells before expansion and post-expansion. Experiments were performed in triplicate. (C) Representative flow cytometric analysis of V δ 1 and V δ 2 expression in CD3⁺ $\gamma\delta$ TCR⁺ cells. Experiments were performed in triplicate. (D) Electron micrograph of $\gamma\delta$ TDEs, revealing the typical morphology and size (50–200 nm). Scale bar: 500 nm. (E) Western blot showing the presence of CD63, weakness of tubulin, and negative of calnexin in $\gamma\delta$ TDEs.

gen-presenting role of $\gamma\delta$ T cells. A large-scale expansion protocol of $\gamma\delta$ T cells has been established,²⁰ making it achievable to obtain large-scale EV production. These characteristics make $\gamma\delta$ T cells potential candidate donors for EV-based drug delivery. The last question is what should be embedded and delivered by $\gamma\delta$ TDEs.

miR-138 has been suggested to function as a tumor suppressor by targeting a set of genes that are relevant to cell migration, epithelial-to-mesenchymal transition (EMT), cell-cycle progression, DNA damage repair, senescence, and differentiation.²¹ Recently, Wei et al.²² demonstrated that miR-138 could target CTLA-4 and programmed cell death 1 (PD-1) in CD4⁺ T cells, resulting in marked glioma tumor regression in immune-competent mice. The direct anti-tumoral and indirect immunoenhancing properties of miR-138 make it a potential candidate for cancer therapy. Due to the multiple potential advantages of $\gamma\delta$ TDEs as a DDS and dual anti-tumoral functions by miR-138, we tested the hypothesis that $\gamma\delta$ TDEs with miR-138 cargo may be an effective therapeutic strategy for OSCC through direct anti-tumoral effects and indirect immunoenhancing effects.

RESULTS

Expanded $\gamma\delta$ T Cells Produce Typical EVs

In order to obtain $\gamma\delta$ TDEs, we initially expanded $\gamma\delta$ T cells *ex vivo* using a well-established zoledronate-dependent protocol.²⁰ During the expansion, typical clusters were formed (Figure 1A), suggesting that $\gamma\delta$ T cells were efficiently stimulated. At the initiation of culture, $\gamma\delta$ T cells accounted for 3%–15% (median 8%) of CD3⁺ cells while increasing to 58%–76% (median 62%) of total population at day 7 before sorting (Figure 1B). After selection and successful induction, the frequency of $\gamma\delta$ T cells reached up to more than 98% of cultured cells at day 14 (Figure 1B). The expanded $\gamma\delta$ T cells are mainly V δ 2 with a percentage ranging from 76% to 96% (median 86%; Figure 1C). The absolute cell number of expanded $\gamma\delta$ T cells increased 360- to 420-fold compared with those before expansion. On day 14, $\gamma\delta$ TDEs were purified from the supernatant of $\gamma\delta$ T cells and then examined by scanning electron microscope, which showed typical rounded particles ranging from 50 to 200 nm in diameter (Figure 1D). The EV

therapeutic effect of human $\gamma\delta$ T cell-based adoptive immunotherapy for solid tumors is drastically needed.⁴

Extracellular vesicles (EVs) are usually named according to their mode of biogenesis and include exosomes that originate from intracellular multivesicular bodies, microvesicles shed from the plasma membrane, and apoptotic bodies that are released by apoptotic cells.¹⁰ Although initially considered to be products of a pathway used to release unwanted material from cells, EVs are now believed to perform a variety of extracellular functions that involve interactions with the cellular microenvironment, such as morphogen signaling, immunological mediation, cell recruitment, and horizontal transfer of genetic material.^{11,12} EVs contain a wide range of functional proteins, mRNAs, and microRNAs (miRNAs)¹³ that allow these structures to operate as signaling platforms for short-range or long-range delivery of information to other cells.¹⁴ As a result, the potential use of EVs as a drug delivery system (DDS) has gained considerable scientific interest.^{15,16} EVs may have multiple advantages over currently available drug delivery vehicles, such as their ability to overcome natural barriers, their intrinsic cell-targeting properties, and stability in the circulation.¹⁵ However, therapeutic applications of EV-based drug delivery are restricted by a lack of ideal EV donor, limited scale of EV production, and inefficient drug cargo.

Because EVs derived from T lymphocytes,¹⁷ dendritic cells (DCs),¹⁸ and natural killer (NK) cells¹⁹ exhibit characteristics and functions from their parent cells, it is reasonable to assume that $\gamma\delta$ T cell-derived EVs ($\gamma\delta$ TDEs) could inherit the direct cytotoxicity and anti-

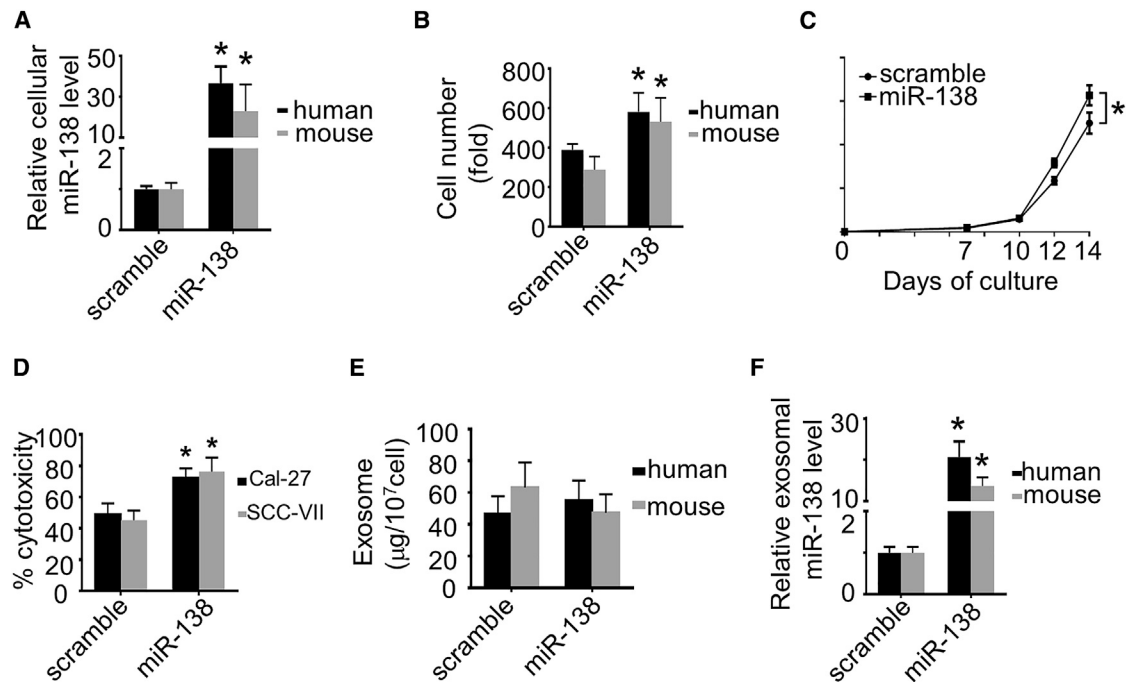


Figure 2. Lentiviral miR-138 Increase Proliferation and Cytotoxicity of $\gamma\delta$ T Cells without Influence on EV Production

(A) miR-138 levels in $\gamma\delta$ T cells were measured by qRT-PCR. Data represent at least three experiments done in triplicate. (B) The absolute cell number of $\gamma\delta$ T cells after lentiviral miR-138 transfection and subsequent expansion. (C) Absolute number of $\gamma\delta$ T cells at the indicated time points. Data represent at least three experiments done in triplicate. (D) The cytotoxicity of $\gamma\delta$ T cells against cancer cells was measured by an LDH cytotoxicity assay with an E:T ratio of 10:1. Data represent at least three experiments done in triplicate. (E) Quantification of EVs derived from scramble miRNA or miR-138-transfected $\gamma\delta$ T cells. Data represent at least three experiments done in triplicate. (F) miR-138 levels in $\gamma\delta$ TDEs were measured by qRT-PCR. Data represent at least three experiments done in triplicate. * $p < 0.05$.

marker CD63 was confirmed to express in $\gamma\delta$ TDEs by western blot (Figure 1E).

Lentiviral miR-138 Increase Proliferation and Cytotoxicity of $\gamma\delta$ T Cells without Influence on EV Production

After purification on day 7, $\gamma\delta$ T cells were infected with lenti-miR-138 virus and further selected and expanded. The levels of miR-138 were significantly increased by lentiviral miR-138 compared with scramble control in $\gamma\delta$ T cells derived from both human PBMCs and mouse spleens (Figure 2A). miR-138 overexpression remarkably induced the expansion of $\gamma\delta$ T cells determined by the total cell number (Figure 2B) and the kinetics of absolute number at the indicated time points (Figure 2C). Moreover, miR-138 overexpression increased the accumulation in S and G2/M phases, and decreased the amount of G1 phase cells (Figure S1A). We analyzed the miR-138 target genes by TargetScan, which revealed 300 target genes of miR-138. The expression profile of these target genes in $\gamma\delta$ T cells and head and neck squamous cell carcinoma (HNSCC) cells was analyzed using two publically available high-throughput datasets, GSE27291 and GSE84557, respectively. We show that 217 out of 300 genes were expressed in $\gamma\delta$ T cells and/or HNSCC cells. Among these 217 genes, 72 genes were highly expressed in $\gamma\delta$ T cells, whereas 64 genes were increased in HNSCC cells (fold change [FC] > 2, false discovery rate [FDR] < 0.01). Gene enrichment analyses demon-

strated that cell cycle is among the top enriched biological processes in HNSCC cells, but not in $\gamma\delta$ T cells (Figures S1B and S1C).

To evaluate the influence of miR-138 overexpression on the cytotoxicity of $\gamma\delta$ T cells against cancer cells, we performed a lactate dehydrogenase (LDH) assay with an effect:target (E:T) ratio of 10:1. As demonstrated in Figure 2D, miR-138 overexpression significantly induced the cytotoxicity of human and mouse $\gamma\delta$ T cells against Cal-27 and SCC-VII cells, respectively, compared with scramble control. We then evaluated the EV amount by quantifying the concentration of exosomal proteins. The miR-138 overexpression in $\gamma\delta$ T cells did not influence the amount of EVs expressed as $\mu\text{g}/10^7$ cells (Figure 2E). Furthermore, the overexpression by miR-138 lentivirus resulted in a mean 19.6-fold and 13.6-fold increase of miR-138 levels in human and mouse $\gamma\delta$ TDEs, respectively (Figure 2F). These results suggest that overexpression of miR-138 with lentivirus in *ex-vivo*-expanded $\gamma\delta$ T cells would obtain miR-138-rich $\gamma\delta$ TDEs accompanying increased expansion and cytotoxicity of $\gamma\delta$ T cells.

miR-138-Rich $\gamma\delta$ TDEs Directly Inhibit the Growth of Tumor

To investigate the role of miR-138-rich $\gamma\delta$ TDEs on tumor viability, Cal-27 cells were treated by miR-138 or scramble control delivered by liposome and $\gamma\delta$ TDEs, respectively. The cell viability of treated Cal-27 cells was measured by CCK-8 assay. We showed that miR-138

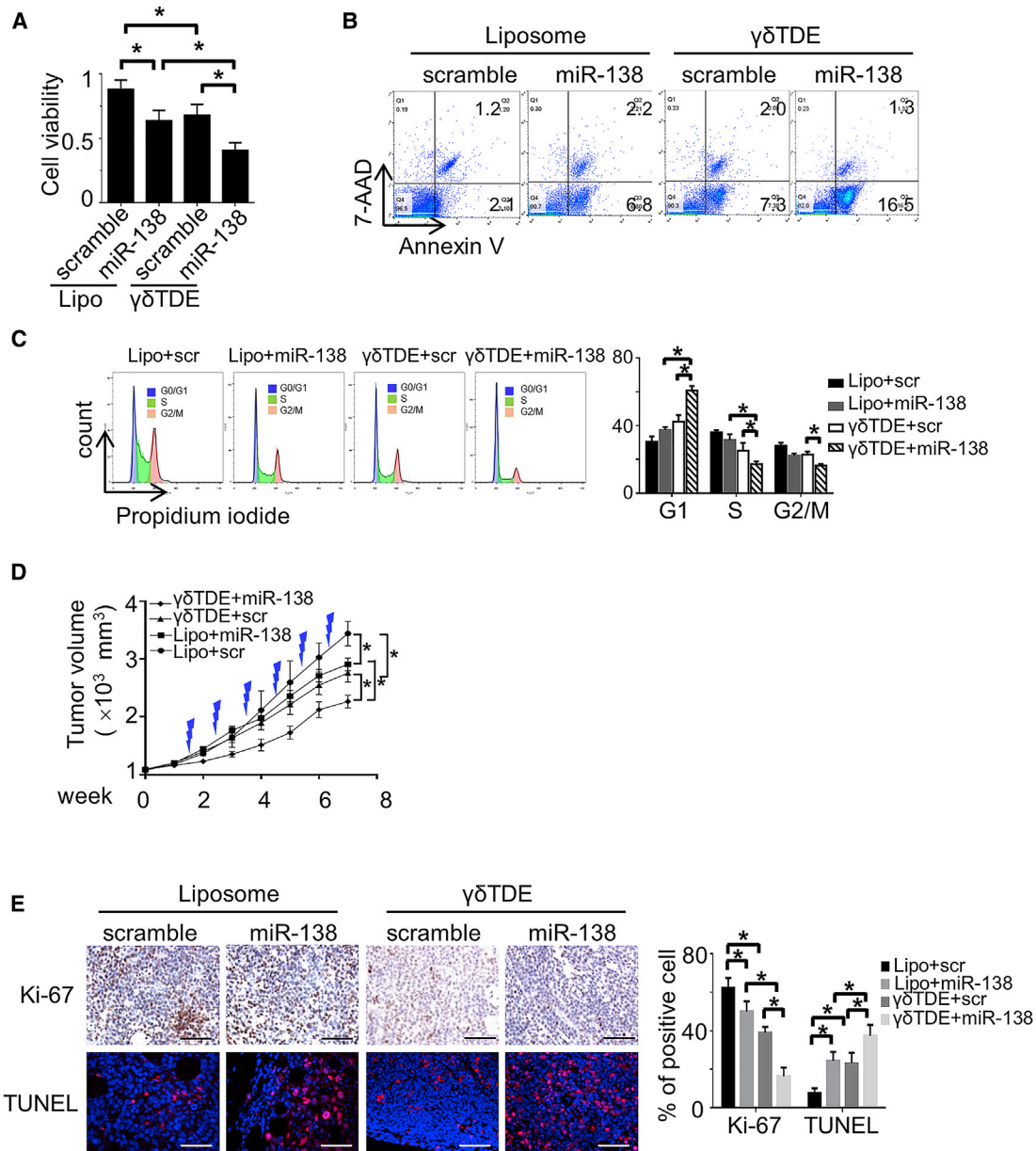


Figure 3. miR-138-Rich $\gamma\delta$ TDEs Directly Inhibit the Growth of Tumor

(A) The viability of OSCC cells treated by liposome and $\gamma\delta$ TDEs carrying either scramble miRNA or miR-138 were measured by CCK-8 assay. Data represent at least three experiments done in triplicate with 10 biological replicates. (B) Representative flow-cytometry-based apoptosis assay of OSCC cells treated by liposome and $\gamma\delta$ TDEs carrying either scramble miRNA or miR-138. Experiments were performed in triplicate. (C) Cell cycle of OSCC cells treated by liposome and $\gamma\delta$ TDEs carrying either scramble miRNA or miR-138 was analyzed by propidium iodide staining and flow cytometry. Data represent at least three experiments done in triplicate. (D) Cal-27 xenograft bearing nude mice received injection of liposome and $\gamma\delta$ TDEs carrying either scramble miRNA or miR-138, respectively. Growth curve of xenograft tumors was monitored. $n = 6$ in each group. (E) Representative image of immunostaining of Ki-67 (upper panel) and TUNEL assay (lower panel) in xenograft tumors. Scale bars: 100 μm . * $p < 0.05$.

and $\gamma\delta$ TDEs, individually, could significantly inhibit the viability of Cal-27 cells. Moreover, delivery of miR-138 by $\gamma\delta$ TDEs had significantly decreased cell viability compared with individual effects of miR-138 and $\gamma\delta$ TDEs (Figure 3A). An apoptosis assay performed with fluorescein isothiocyanate (FITC)-Annexin V/7-aminoactinomy-

cin D (7-AAD) confirmed that miR-138-rich $\gamma\delta$ TDEs induced more apoptosis of cancer cells than miR-138 and $\gamma\delta$ TDEs independently (Figure 3B). Cell-cycle distribution of OSCC cells treated by $\gamma\delta$ TDEs was further performed. Compared with liposome-transfected miR-138 and scramble-cargo $\gamma\delta$ TDEs, miR-138-rich $\gamma\delta$ TDE significantly

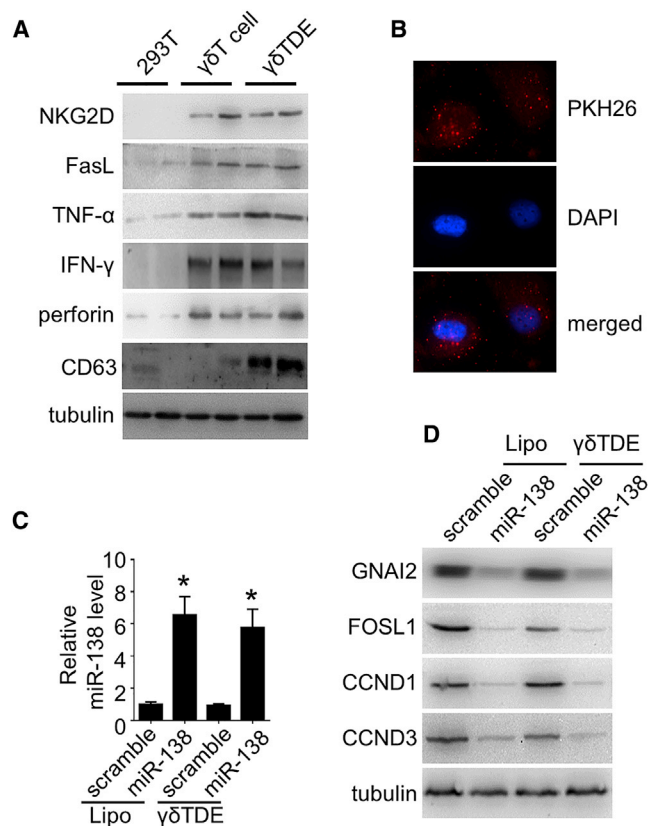


Figure 4. $\gamma\delta$ TDEs Inherit the Cytotoxic Profiles of $\gamma\delta$ T Cells

(A) Cytotoxic markers of $\gamma\delta$ T cells were measured by western blot with 293T cells serving as control. (B) Representative fluorescence microscopy image showing the internalization of PKH26-labeled (red) $\gamma\delta$ TDEs by OSCC cells. (C) miR-138 levels in OSCC cells treated by liposomes or $\gamma\delta$ TDEs were measured by qRT-PCR. Data represent at least three experiments done in triplicate. * $p < 0.05$. (D) The representative targets of miR-138 in OSCC cells were measured by western blot.

decreased the accumulation of Cal-27 cells in S and G2/M phases, and increased the amount of G1 phase cells (Figure 3C).

We next sought to investigate the *in vivo* effects of $\gamma\delta$ TDEs on tumor growth. To rule out the potential interference of immune effects of $\gamma\delta$ TDEs, the immunodeficient nude mice were applied to establish xenografts with Cal-27 cells. Liposome and $\gamma\delta$ TDEs (10 μ g) were injected to the xenografts twice a week for a total of 6 weeks. In parallel with *ex-vivo* results, liposome-transfected miR-138 and scramble miRNA $\gamma\delta$ TDEs could reduce the growth of xenograft tumors compared with liposome + scramble miRNA. Mice that received miR-138-rich $\gamma\delta$ TDEs treatment kept a much slower growth than other groups during the whole period (Figure 3D). The xenograft tumors were then harvested for histological analyses. Frozen sections were observed under fluorescence microscope for the GFP-positive cells that represent successful exogenous miRNA delivery. A higher frequency of GFP⁺ cells was observed in mice that had $\gamma\delta$ TDEs as delivery vesicle for miR-138 (Figure S2A). However, liposome and

$\gamma\delta$ TDE delivery had equal miR-138 distribution in spleen, brain, lung, kidney, and liver (Figure S2B). The proliferation of tumor cells was detected by IHC staining of Ki-67, and the apoptosis was measured by TUNEL assay. Mice that received miR-138-rich $\gamma\delta$ TDE treatment had remarkably decreased Ki-67 staining (Figure 3E, left upper panel) and increased TUNEL staining (Figure 3E, left lower panel) compared with those that received either liposome-transfected miR-138 or scramble-cargo $\gamma\delta$ TDEs.

These results suggest that both miR-138 and $\gamma\delta$ TDEs, individually, have direct anti-tumor effects, and that therapeutic outcome of OSCC may benefit from delivering miR-138 by $\gamma\delta$ TDEs.

$\gamma\delta$ TDEs Inherit the Cytotoxic Profiles of $\gamma\delta$ T Cells

Because $\gamma\delta$ TDEs, independently, could inhibit the growth of tumor cells without carrying miR-138, we measured the expression of cytotoxic markers of $\gamma\delta$ T cells in $\gamma\delta$ TDEs by western blot. Our data showed positive expression of NKG2D, Fas ligand (FasL), tumor necrosis factor alpha (TNF- α), interferon- γ (IFN- γ), and perforin in $\gamma\delta$ T cells, as well as in $\gamma\delta$ TDEs, but not in 293T control cells (Figure 4A). $\gamma\delta$ TDEs were labeled with fluorescent PKH26 and then co-incubated with OSCC cells. The PKH26-labeled $\gamma\delta$ TDEs were visualized to be internalized by Cal-27 cells after 2-hour incubation measured by a fluorescence microscope (Figure 4B). We then measured the miR-138 expression in the recipient OSCC cells treated by liposome and $\gamma\delta$ TDEs, respectively. The qRT-PCR revealed that both liposome and $\gamma\delta$ TDEs could efficiently deliver miR-138 to the Cal-27 cells with 6.6-fold and 5.8-fold increase, respectively (Figure 4C). We next investigated whether miR-138 regulates its target genes in recipient cells. miR-138 delivered by liposome and $\gamma\delta$ TDEs significantly decreased the expression of selected miR-138 targets, GNAI2, FOSL1, CCND1, and CCND3, determined by western blot (Figure 4D). These represented targets of miR-138 are involved in the regulation of cell proliferation and cell cycle. These results suggest that $\gamma\delta$ TDEs, inheriting the cytotoxic profile of $\gamma\delta$ T cells, could efficiently deliver miR-138 to cancer cells to serve as a cancer suppressor.

miR-138-Rich $\gamma\delta$ TDEs Stimulate Anti-tumor Immunity

Activated $\gamma\delta$ T cells have been suggested to display phenotypic characteristics of APCs and to induce the cytotoxicity of CD8⁺ T lymphocytes.^{7,23} No study, to the best of our knowledge, has reported whether $\gamma\delta$ TDEs could inherit the antigen-presenting function of $\gamma\delta$ T cells. We therefore sought to investigate whether miR-138-rich $\gamma\delta$ TDEs can modulate the anti-tumor immunity. Immunodeficient nude mice and immune-competent C3H mice received intravenous (i.v.) injection of either liposome or $\gamma\delta$ TDEs with or without miR-138 cargo, respectively. Twenty-four hours after the sixth immunization, 1×10^7 SCC-VII cells were subcutaneously injected, and tumor growth was monitored weekly. The xenograft tumors were then harvested for histological analyses. Fluorescence microscope showed that no remarkable GFP⁺ cell (exogenous miRNA-transfected cell) was observed in tumors harvested from mice that received either liposome or $\gamma\delta$ TDE vaccination (Figure S2C). Compared with liposome, $\gamma\delta$ TDEs (even with scramble miRNA) could significantly inhibit

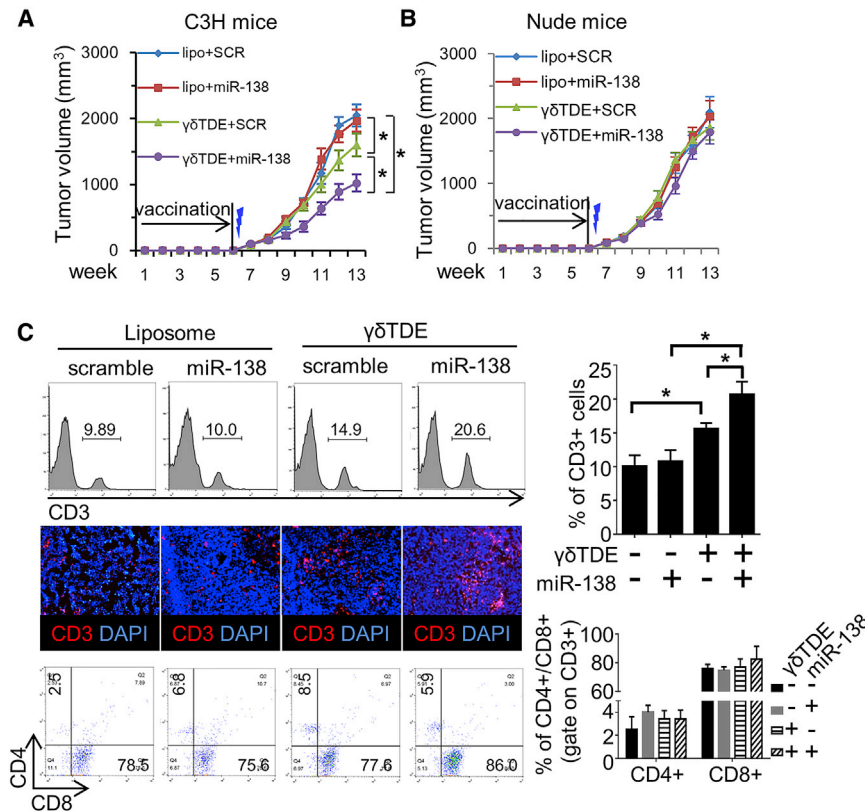


Figure 5. miR-138-Rich $\gamma\delta$ TDEs Stimulate Anti-tumor Immunity

C3H mice (A) and nude mice (B) received weekly i.v. injection of either liposome or $\gamma\delta$ TDEs for 6 weeks. Twenty-four hours after the sixth immunization, 1×10^7 SCC-VII cells were subcutaneously injected, and tumor growth was monitored weekly. $n = 6$ in each group. Thunderbolt indicates subcutaneous (s.c.) injection of cancer cells. (C) Representative flow cytometry analysis (left upper panel) and immune-fluorescence staining (left middle panel) showing the infiltration of CD3⁺ lymphocytes in the tumor on C3H mice. Flow cytometry analysis (left bottom panel) of CD4⁺ and CD8⁺ T cells in the CD3⁺ population. Quantitative analysis of flow cytometry data of CD3⁺ T cells (right upper panel) and CD4⁺/CD8⁺ T cells (right lower panel). * $p < 0.05$.

the growth of tumor in immunocompetent C3H mice. Although delivery by liposome had no influence on the tumor growth, miR-138 embedded by $\gamma\delta$ TDEs further decreased the growth of tumor compared with $\gamma\delta$ TDEs alone (Figure 5A). In nude mice, however, tumor growth was not different between any vaccinating strategies (Figure 5B). These results suggest that the effect of $\gamma\delta$ TDEs and their miR-138 cargo on tumor growth suppression was immunity dependent.

The tumors in C3H mice were harvested and analyzed for the infiltration of CD3⁺ T lymphocytes. The flow cytometry analysis showed that liposome has no effect on the infiltration of CD3⁺ T cells no matter whether scramble or miR-138 was packaged in. Compared with liposome, $\gamma\delta$ TDEs significantly increased the recruitment of CD3⁺ T cells. Intriguingly, miR-138 delivered by $\gamma\delta$ TDEs further increased CD3⁺ T cell recruitment (Figure 5C). The immunofluorescence staining confirmed the increased infiltration of CD3⁺ T cells by miR-138 and $\gamma\delta$ TDEs. The percentage of CD4⁺ and CD8⁺ in the total CD3⁺ T cells was not different between groups. These results suggest that miR-138 and $\gamma\delta$ TDEs collaborate in the anti-tumor immunity regulation.

miR-138-Rich $\gamma\delta$ TDEs Regulate Anti-tumor Immunity by CD8⁺ T Cells

We measured the expression of antigen-presenting MHC class II molecules, as well as T cell co-stimulation and adhesion molecules,

on $\gamma\delta$ T cells and $\gamma\delta$ TDEs using western blot with 293T cells serving as a negative control. MHC class II molecular CD80, CD86, and CD40 were found to express on both $\gamma\delta$ T cells and $\gamma\delta$ TDEs, but not 293T cells. MHC class I weakly expressed on 293T cells and was remarkably upregulated on both $\gamma\delta$ T cells and $\gamma\delta$ TDEs. In addition, none of the co-stimulatory markers investigated were remarkably affected by miR-138 KD in either $\gamma\delta$ T cells or $\gamma\delta$ TDEs (Figure 6A). These results suggest that $\gamma\delta$ TDEs inherit the antigen-presentation characteristics by their parent $\gamma\delta$ T cells. The PKH26-labeled $\gamma\delta$ TDEs were labeled with fluorescent PKH26 and then co-incubated with CD8⁺ T cells. The PKH26-labeled $\gamma\delta$ TDEs were internalized by CD8⁺ T cells after 24-hour incubation measured by a fluorescence microscope (Figure 6B). The miR-138 expression in the recipient CD8⁺ T cells treated by liposome and $\gamma\delta$ TDEs was measured by qRT-PCR. $\gamma\delta$ TDEs, but not liposome, efficiently delivered miR-138 and significantly increased the miR-138 expression in the recipient CD8⁺ T cells (Figure 6C). To study the role of $\gamma\delta$ TDEs and miR-138 on CD8⁺ T cell proliferation, we stained CD8⁺ T cells by carboxyfluorescein succinimidyl ester (CFSE) and co-incubated with either $\gamma\delta$ TDEs or liposome for 6 days. $\gamma\delta$ TDEs significantly increased the proliferation of CD8⁺ T cells, which was further remarkably increased by their miR-138 cargo. Liposome, no matter whether scramble miRNA or miR-138 was carried, has no effect on CD8⁺ T cell proliferation (Figure 6D). Consistently, the IFN- γ production by CD8⁺ T cells was measured by ELISpot assay, which showed that $\gamma\delta$ TDEs significantly induced the IFN- γ production. $\gamma\delta$ TDEs with miR-138 cargo had significantly increased IFN- γ levels compared with scramble miRNA cargo (Figure 6E). Flow cytometry analysis further validated the increased IFN- γ expression by CD8⁺ T cells treated with $\gamma\delta$ TDEs with miR-138 cargo (Figure 6F). We then performed a cytotoxicity assay to assess the cytotoxic activity of $\gamma\delta$ TDE-treated CD8⁺ T cells against OSCC cells. As shown in Figure 6F, $\gamma\delta$ TDEs with scramble miRNA could induce a significant

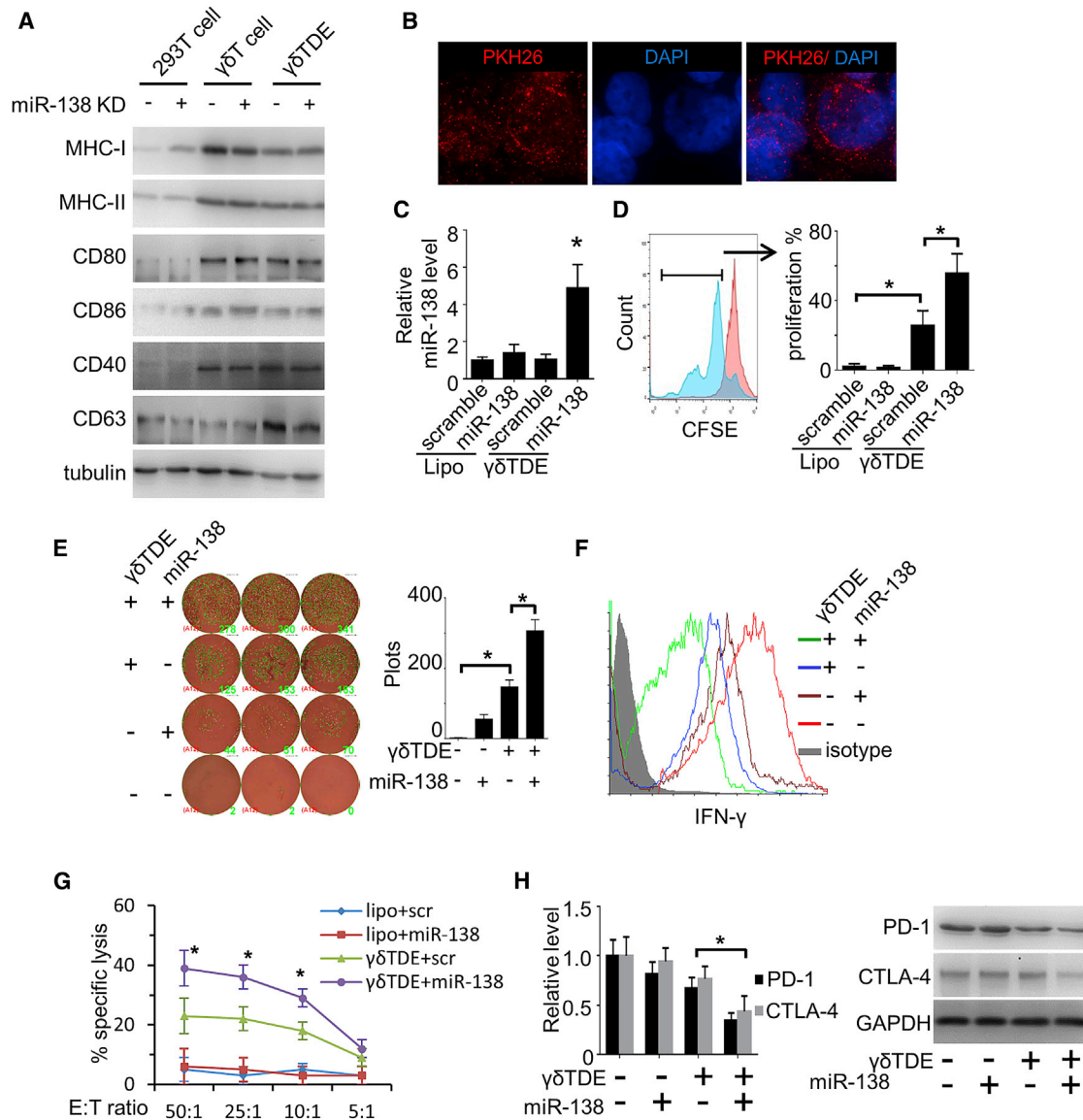


Figure 6. miR-138-Rich $\gamma\delta$ TDEs Regulate Anti-tumor Immunity by CD8⁺ T Cells

(A) Antigen-presenting markers of $\gamma\delta$ T cells were measured by western blot with 293T cells serving as control. (B) Representative fluorescence microscopy image showing the internalization of PKH26-labeled (red) $\gamma\delta$ TDEs by CD8⁺ T cells. (C) miR-138 levels in CD8⁺ T cells treated by liposomes or $\gamma\delta$ TDEs were measured by qRT-PCR. Data represent at least three experiments done in triplicate. (D) CD8⁺ T cells were pre-labeled with CFSE and then incubated with liposomes or $\gamma\delta$ TDEs at the presence of IL-2. CFSE⁺ cells were measured by flow cytometry. Data represent at least three experiments done in triplicate. (E) IFN- γ production by CD8⁺ T cells was measured by ELISpot assay. (F) The production of IFN- γ by CD8⁺ T cells was measured by flow cytometry. The CD8⁺ population was gated for IFN- γ analysis. Experiments were performed in triplicate. (G) The cytotoxicity of liposome or $\gamma\delta$ TDE-treated CD8⁺ T cells against OSCC cells was measured by an LDH cytotoxicity assay with E:T ratios of 50:1, 25:1, 10:1, and 5:1. Data represent at least three experiments done in triplicate. (H) PD-1 and CTLA-4 expression on the mRNA level (left panel) and protein level (right panel) were measured by qRT-PCR and western blot, respectively. Data represent at least three experiments done in triplicate. *p < 0.05.

increase of CD8⁺ T cell cytotoxicity, which was further increased by $\gamma\delta$ TDEs carrying miR-138 (Figure 6G). Because immune checkpoint molecules PD-1 and CTLA-4 have been reported to be miR-138 targets, we measured PD-1 and CTLA-4 expression in CD8⁺ T cells by qRT-PCR and western blot, respectively. $\gamma\delta$ TDEs with miR-138 cargo significantly decreased the expression of PD-1 and CTLA-4

at both mRNA (Figure 6G, left panel) and protein levels (Figure 6H, right panel). These results suggest that both miR-138 and $\gamma\delta$ TDEs, individually, have immunostimulatory effects on CD8⁺ T cells, and that a combination of miR-138 and $\gamma\delta$ TDEs could achieve an additive effect, making miR-138-rich $\gamma\delta$ TDE a candidate for OSCC therapy.

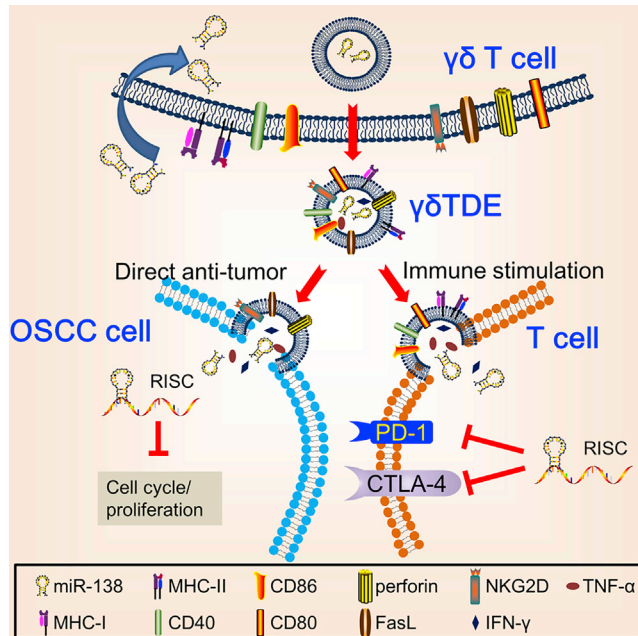


Figure 7. Schematic Cartoon Illustrates Dual Anti-tumoral Functions by miR-138-Rich $\gamma\delta$ TDEs

DISCUSSION

$\gamma\delta$ T cells are suggested to have direct cytotoxicity against a wide range of cancer types in a manner similar to NK cells and can stimulate expansion of cytotoxic effector T cells by mimicking the functions of DCs.^{6,7,24} The dual functions of $\gamma\delta$ T cells make them attractive candidates for cancer immunotherapy.²⁵ EVs have emerged as potential tools for DDS due to the fact that they are naturally produced with expected organ tropism and low side effect.^{15,26} However, to the best of our knowledge, no study has ever applied $\gamma\delta$ TDEs as DDS. In the present study, we demonstrated that $\gamma\delta$ TDEs, inheriting NK- and DC-like profiles of parent $\gamma\delta$ T cells, could efficiently inhibit the growth of OSCC with miR-138 cargo, which can function as tumor suppressor and immune enhancer on the other hand (Figure 7). Our results suggest that an integration of $\gamma\delta$ TDEs and miR-138 could serve as a therapeutic candidate for OSCC.

In the present study, we show that $\gamma\delta$ TDEs inherit the profiles of $\gamma\delta$ T cells, having direct anti-tumor effects on OSCC and stimulation on anti-tumor immunity. This is the first study, to the best of our knowledge, to demonstrate the anti-tumor function of $\gamma\delta$ TDEs. It has been reported that EVs derived from NK cells not only express both typical NK markers (i.e., CD56) and killer proteins (i.e., FasL and perforin), but also exert antitumor and immune homeostatic activities.^{19,27} Consistently, T cell-derived EVs contain TCR subunits, Src-like tyrosine kinases, and adhesion molecules.²⁸ Moreover, DC-derived EVs express functional MHC class I, MHC class II, and T cell costimulatory molecules, which prime specific cytotoxic T lymphocytes against murine tumors.²⁹ The profiles of $\gamma\delta$ TDEs described in our study

further support the notion that EVs vary between cell types, reflecting the specific functions of their parent cells to a certain extent.¹⁷

Due to the intrinsic role of EVs in endogenous gene transfer in both biological and pathological settings, the nascent era of EV-based DDS has been rapidly growing. Perhaps the most tantalizing and ambitious applications for EVs as DDS are their potential to help realize the enormous opportunities for gene and biologic therapies in oncology, which has been a long-standing challenge because of the lack of appropriate carriers.³⁰ Cancer-derived EVs have been described to function as natural carriers that can efficiently deliver CRISPR/Cas9 plasmids to cancer, resulting in the induction of apoptosis in ovarian cancer and enhancement of chemosensitivity to cisplatin.³¹ Several other preclinical studies have investigated the delivery efficiency by EVs derived from mesenchymal stem cells (MSCs),³² macrophages,³³ NK cells,²⁷ and erythrocytes³⁴ in cancer treatment with encouraging results. Clinical trials that utilized DC-derived EVs to treat advanced melanoma³⁵ and non-small cell lung cancer patients³⁶ demonstrated partial immunological and clinical responses, but survival benefits were largely variable and limited. MSCs are multiple precursors with the ability to locate and migrate toward damaged and inflammatory microenvironments, such as solid tumors. This property makes them a candidate for therapeutic agent delivering.³⁷ MSC-EVs have been demonstrated to recapitulate the therapeutic potential of MSCs on glioma through delivering exogenous miR-146b.³⁸ However, MSC-EVs have also shown to have heterogeneous effector mechanisms as MSCs. For instance, MSC-EVs enhanced vascular endothelial growth factor (VEGF) expression in tumor cells by activating extracellular signal-regulated kinase 1/2 (ERK1/2) pathway and promoted tumor growth *in vivo*.³⁹ In addition, NK cells release EVs expressing typical protein markers of NK cells and containing killer proteins (i.e., Fas ligand and perforin molecules).⁴⁰ NK-EVs have been demonstrated to exert cytotoxic effects on different human tumor cells.^{27,40} However, to the best of our knowledge, no study has evaluated the potential application of NK-EV as a DDS in the cancer treatment. According to our results, we suggest that $\gamma\delta$ TDEs may serve as an efficient DDS in cancer therapy attributing to several advantages: (1) $\gamma\delta$ TDEs inherit the NK-like profile of $\gamma\delta$ T cells independently on MHC molecules, (2) $\gamma\delta$ TDEs could inherit APC-like function of $\gamma\delta$ T cells, and (3) large-scale *ex-vivo* expansion protocol of $\gamma\delta$ T cells has been established. Such advantages include the specificity of delivery to cancer cells and T lymphocytes with abilities to direct target cancer cell and indirect effects on anti-cancer immunity improvement.

Although EVs as DDS are still in their infant stage, liposomes have gained popularity for applications as drug carriers. Synthetic liposomes are easy to manufacture, allowing advantageous simplicity in isolation and high yield. However, the high toxicity, lack of targeting specificity, and rapid elimination from the circulation have hindered their wide application.⁴¹ Our results showed that liposomes failed to transfect miR-138 to T cells either *in vivo* or *in vitro*, whereas $\gamma\delta$ TDEs can efficiently deliver miR-138 to T cells, suggesting higher delivery efficiency by $\gamma\delta$ TDEs than liposomes in T cell targeting. Indeed,

T cells are particular about the EVs to be incorporated, because it has been reported that T cells prefer a surface contact with tumor-derived EVs rather than internalizing them.⁴² Given that $\gamma\delta$ TDEs can efficiently be internalized by T cells, we suggest that $\gamma\delta$ TDEs are efficient DDSs to transport drugs and nuclear acids to T cells rather than tumor-derived EVs. But the efficiency between $\gamma\delta$ TDEs and EVs derived from other cell types, e.g., DCs, NK cells, and MSCs, needs to be explored further.

The clearance of EVs in the circulation by monocytes and macrophages might be a concern in the application of EVs as drug delivery vesicles. Compared with cell-based therapy, EVs may have a shorter lifetime in the circulation. The persistence of tumor-killing capacity of cell-based therapy depends on their own lifespan and further *in vivo* expansion, whereas the extent of cytokine release from cell-based therapy (e.g., chimeric antigen receptor-based T cell adoptive immunotherapy) and the status of *in vivo* expansion of these cells cannot be appropriately controlled, which is the potential source of adverse events, such as cytokine release syndrome and “on-target, off-tumor” response.⁴³ The cell-free nature and biological properties of EVs make them an attractive replacement of cell-based therapy with advantages such as controllable cytokine release syndrome, well penetration within solid tumor, and easy modification.⁴³ Moreover, Kamerkar et al.⁴⁴ demonstrated an enhanced retention of EVs, compared with liposomes, in the circulation due to CD47-mediated protection of EVs from phagocytosis by monocytes and macrophages. These results suggest that EVs could serve as an attractive replacement of cell-based therapy with drug-delivering property. miR-138, as a tumor suppressor, has been consistently downregulated in OSCCs^{45–47} and many other cancer types as well.^{21,48} The experimentally validated miR-138 target genes play essential roles in the initiation and progression of cancer, including cell migration (e.g., ZEB2, HIF-1 α), EMT (e.g., TWIST2, EZH2), cell-cycle regulation (e.g., CCND1, CCND3, FOSL1), DNA damage and repair (e.g., H2AX, XRCC1), and senescence (e.g., Sirt1, TERT).²¹ By regulating these target genes, miR-138 can inhibit proliferation and invasion, induce apoptosis, and enhance chemosensitivity of many cancer types.⁴⁸ More recently, miR-138 has been uncovered by its participation in immune regulation. Wei et al.²² demonstrated *in vivo* miR-138 treatment of GL261 gliomas in immune-competent mice resulted in remarked tumor regression through directly targeting immune checkpoints CTLA-4 and PD-1 in CD4⁺ T cells, suggesting miR-138 as a novel immunotherapeutic agent for glioma. Considering the multiple mechanisms by which miR-138 utilizes to inhibit cancer growth, we chose miR-138 as the “drug cargo” of $\gamma\delta$ TDEs and proved its dual effects on direct anti-tumor effects and indirect immunity enhancement in OSCC xenograft models.

Given that miR-138 targets genes involved in cell proliferation and cell cycle, the loading of miR-138 to $\gamma\delta$ T cells has a potential inhibition on $\gamma\delta$ T cell proliferation and $\gamma\delta$ TDE production. There is no evidence, to the best of our knowledge, to indicate any suppression by miR-138 on T cell function. In addition to the aforementioned role on CD4⁺ T cell immunoenhancement through targeting CTLA-4

and PD-1,²² miR-138 has been also suggested to regulate Th1/Th2 balance in CD4⁺ T cells through targeting RUNX3.⁴⁹ In our present study, miR-138 overexpression in $\gamma\delta$ T cells remarkably increased the expression of miR-138 in both $\gamma\delta$ T cells and $\gamma\delta$ TDEs with moderate increased $\gamma\delta$ T cells proliferation, but no influence on $\gamma\delta$ TDE production. In addition, gene enrichment analyses demonstrated that cell cycle is among the top enriched biological process in HNSCC cells, but not in $\gamma\delta$ T cells, which might be the reason that miR-138 overexpression in OSCC cells caused proliferation inhibition rather than $\gamma\delta$ T cells. These results suggest that miR-138 could be an ideal “bullet” loaded in $\gamma\delta$ T cells for cancer therapy.

In conclusion, we showed in the present study that miR-138-rich $\gamma\delta$ TDEs achieved synergetic therapeutic effects on OSCC compared with miR-138 and $\gamma\delta$ TDEs alone, which is benefited from the individual direct anti-cancer effects on OSCC and immunostimulatory effects on T cells by both $\gamma\delta$ TDEs and miR-138. In addition, $\gamma\delta$ TDEs could serve as an efficient DDS for miRNAs in the treatment of cancer.

MATERIALS AND METHODS

Human and animal studies have been approved by the Institutional Ethics Committee of Sichuan Cancer Hospital (approval no. KY-2017-017-01). Peripheral blood samples were obtained from healthy volunteers without any malignancy. Informed consent was obtained from all donors prior to blood collection.

$\gamma\delta$ T Cell Culture

Human $\gamma\delta$ T cells were expanded and cultured from human PBMCs as described previously.⁵⁰ In brief, whole blood (7.5–8 mL) was collected in a BD vacutainer CPT cell preparation tube with sodium heparin (BD, Franklin Lakes, NJ, USA) and centrifuged to isolate PBMCs at the interphase. Murine $\gamma\delta$ T cells were expanded from splenocytes of C3H mice. Human PBMCs or mouse splenocytes were then cultured in AIM V medium (Thermo Fisher Scientific, Waltham, MA, USA) with recombinant interleukin-2 (IL-2; R&D Systems, Minneapolis, MN, USA) and zoledronate (Aclasta, Novartis, Switzerland) to final concentrations of 1,000 IU/mL and 5 μ M, respectively, at the presence of tumor conditioned medium. On day 7, $\gamma\delta$ T cells were sorted using a MoFlo XDP cell sorter (Beckman Coulter, Brea, CA, USA).

Sorted $\gamma\delta$ T cells were seeded in a 24-well plate and infected with LV-hsa-mir-138 (GENECHEM, Shanghai, China) with 5 μ g/mL polybrene, and stable clones were selected and maintained in medium described above with 0.5 μ g/mL puromycin.

EV Isolation, Quantification, Labeling, and RNA Extraction

Ten microliters of culture media was mixed with ExoQuick EV precipitation solution, and EV isolation was performed according to the manufacturer's instructions (SBI System Biosciences, CA, USA) as described previously.⁵¹ The ExoQuick/biofluid mixture was centrifuged at 1,500 \times g for 30 min, and the precipitated EVs were re-suspended in nuclease-free water. After re-suspension of precipitated

EVs, the concentration of proteins contained in EVs was quantified using bicinchoninic acid assay (BCA; Pierce, Rockford, IL, USA); EV quantities are therefore expressed as micrograms of containing proteins as described by Roccaro et al.⁵²

Purified EVs were labeled with the red fluorescent linker PKH26 (Sigma-Aldrich, St. Louis, MO, USA) as described previously.⁴² For *in vitro* EV treatment studies, equal amounts of EVs (micrograms of proteins) were added into the medium at a concentration of 10 µg/mL. To extract total RNA, an equal quantity of EV particles was lysed using RNeasy mini kit (QIAGEN, Germantown, MD, USA), then 5 µg of cel-miR-39 was added into the lysate as a spike-in control. Total RNA isolation was done according to the manufacturer's protocol. EVs used for *in vivo* experiments were prepared with an ultracentrifugation protocol as described previously.⁴²

qRT-PCR

Total RNA was reverse transcribed using the TaqMan MicroRNA Reverse Transcription Kit (Applied Biosystems). Quantification of miR-138 was performed with predesigned TaqMan microRNA assays on an ABI PRISM 7700 sequence detection system (Applied Biosystems, Foster City, CA, USA). For mRNA quantification, total RNAs were reverse transcribed using first-strand cDNA synthesis Kit (Invitrogen, Carlsbad, CA, USA) following the manufacturer's instructions. PCR was performed using TaqMan universal PCR master mix (Applied Biosystems) on an ABI PRISM 7700 sequence detection system (Applied Biosystems). PCR conditions were 50°C for 2 min, followed by incubation at 95°C for 10 min, then 40 cycles of two-step PCR, including denaturing at 95°C for 15 s and annealing and extension at 60°C for 60 s. Reactions were run in triplicate, and the results were averaged. Relative expression was calculated using the $\Delta\Delta C_t$ method after normalization to cel-miR-39 and glyceraldehyde 3-phosphate dehydrogenase (GAPDH), respectively, for miRNA and mRNA quantification. Primers and probes for PD-1 and CTLA-4 were described previously.⁵³

LDH Release Assay

To determine the cytotoxicity of T cells, we performed the LDH assay with an LDH cytotoxicity assay kit (Thermo Fisher Scientific) following the manufacturer's protocol. In brief, T cells (effect cells) and target cells (Cal-27 and SCC-VII) were co-cultured at the ratios of 50:1, 25:1, 10:1, and 5:1. The LDH released into the medium is transferred to a new plate and mixed with Reaction Mixture. After 30-min room temperature incubation, LDH activity was determined at 490 nm in a plate-reading spectrophotometer: % cytotoxicity = $([\text{experimental value} - \text{effector cells spontaneous control} - \text{target cells spontaneous control}] / [\text{target cell maximum control} - \text{target cells spontaneous control}]) \times 100$.

CCK-8 Assay

To evaluate the inhibitory effects of $\gamma\delta$ TDEs on OSCC cells, we cultured Cal-27 and SCC-VII cells (5,000 cells/well) in 96-well plates and incubated with 10 µg of $\gamma\delta$ TDEs for 24 hr. CCK-8 solution (10 µL/well; Beyotime, Shanghai, China) was added to the cells. After

a 4-hr incubation, absorbance at 450 nm was measured using a microplate reader (Thermo Fisher Scientific).

Flow Cytometry

Single-cell suspensions were prepared from cultured cells or fresh tumor tissues. Red cells were removed using ammonium chloride lysis buffer when necessary. 1×10^6 cells were incubated at 4°C for 30 min with different combinations of fluorescent-conjugated antibodies for $\gamma\delta$ T cells (anti-V γ 9 TCR-allophycocyanin [BioLegend, San Diego, CA, USA], anti-CD3-PECy7 [BioLegend], anti-V δ 2 TCR-peridinin chlorophyll [PerCP]-Cy5.5 [BioLegend], and anti-V δ 1 TCR-FITC [Thermo Fisher Scientific]), T cells (FITC-anti-CD4 [BD Biosciences, San Jose, CA, USA], PE-anti-CD8 [BD Biosciences], and PE/Cy7-anti-CD3 [BioLegend]). For intracellular staining of IFN- γ , cells were incubated with staphylococcal enterotoxin B for 6 hr in the presence of 19 brefeldin A as described by the manufacturer (BD Biosciences, San Jose, CA, USA). Cells were then stained with IFN- γ PerCP-Cy5.5 (BD Biosciences).

For $\gamma\delta$ TDE-mediated cell proliferation experiments, CD8⁺ T cells were stained with CFSE (4.5 mM) at 37°C for 20 min. The labeled cells were cultured in AIM V Medium with IL-2 and zoledronate at the presence of $\gamma\delta$ TDE derived from different conditions for 6 days. Cells were harvested, and CFSE was measured by a flow cytometer with 488 nm excitation and emission filters.

Apoptosis Assay

An FITC-Annexin V/7-AAD (Thermo Fisher Scientific) double-staining protocol was applied to measure the cytotoxic effects of $\gamma\delta$ TDEs against OSCC cells as described previously. Cal-27 and SCC-VII cells were treated by 10 µg of $\gamma\delta$ TDEs for 24 hr. OSCC cells were washed twice with PBS, centrifuged to remove the debris, and resuspended in binding buffer at a concentration of 1×10^6 cells/mL. Cells were stained with 5 µL of FITC-Annexin V and 5 µL of 7-AAD for 15 min at room temperature in the dark. After binding buffer (0.4 mL) being added, cells were analyzed using a BD FACSCanto II flow cytometer.

Cell Cycle

Cells were trypsinized, washed with PBS, and fixed in cold 70% ethanol for 30 min. After wash, cells were resuspended in 0.5 mL of PBS containing 0.25% Triton X-100 and incubated on ice for 15 min. Cells were then stained with propidium iodide (20 µg/mL) at the presence of 10 µg/mL RNase A at room temperature in the dark for 30 min. Flow cytometry was performed using a BD FACSCanto II flow cytometer. Cell cycle was analyzed in FlowJo software (FlowJo, Ashland, OR, USA).

Western Blot

Total protein was isolated from EVs and cultured cells with a radioimmunoprecipitation assay (RIPA) lysis and extraction buffer (Thermo Fisher Scientific), and protein concentrations were detected by a BCA protein assay kit (Pierce, Rockford, IL, USA). Thirty micrograms of proteins from each sample was separated on an 8%

SDS-PAGE gel and electrophoretically transferred to polyvinylidene fluoride (PVDF) membranes (Millipore, Boston, MA, USA). Membranes were blocked with 2% BSA in TBS containing 0.1% Tween 20 at 37°C for 2 hr and then incubated for 2 hr with either CD63 (Santa Cruz, CA, USA), Calnexin (Cell Signaling Technology), NKG2D (R&D Systems), FasL (R&D Systems), TNF- α (NOVUS, Littleton, CO, USA), IFN- γ (NOVUS), perforin (Invitrogen), tubulin (NOVUS), MHC class I (Abnova, Beijing, China), MHC class II (NOVUS), CD80 (Bio-Rad Laboratories, Hercules, CA, USA), CD86 (R&D Systems), and CD40 (R&D Systems). Horseradish peroxidase-conjugated anti-mouse or anti-rabbit IgG was used as a secondary antibody (diluted 1:5,000 in TBST with 2% BSA and incubated for 1 hr). Bands were scanned using a densitometer (GS-700; Bio-Rad Laboratories), and quantification was performed using Quantity One 4.4.0 software.

Xenograft

The immunodeficient nude mice and immunocompetent C3H mice (females, 6–8 weeks of age) were obtained from Charles River (Beijing, China). Tumor cells were injected subcutaneously (1×10^7 cells/200 μ L PBS/mouse) into the back of mice. In the EV injection experiments, 10 μ g of EVs was i.v. injected into the tail vein of mice. The tumor size was monitored weekly by measuring diameters using vernier calipers and calculated as $\pi l s^2/6$, where l = the long side and s = the short side. Mice were euthanized at week 7.

ELISpot

An IFN- γ ELISpot kit was applied (BD, Franklin Lakes, NJ, USA) according to the manufacturer's instructions. In brief, 1×10^4 T cells were seeded in BD ELISpot plate coated with anti-mouse IFN- γ and cultured with anti-mouse IL-2 and liposome/ $\gamma\delta$ TDEs for 48 hr at 37°C. After incubation, plates were washed and incubated with biotinylated anti-mouse IFN- γ in detection antibody solution for 2 hr. After wash, 100 μ L/well streptavidin-horseradish peroxidase (HRP) solutions were added to each well and incubated for 1 hr. 3-Amino-9-ethylcarbazole (AEC) substrate solution was then added and spots were counted with an AID ELISpot Reader system using ELISpot Reader v6.0. T cells alone in duplicate wells served as the background control.

Expression Analysis of miR-138 Target Genes in $\gamma\delta$ T Cells and HNSCC Cells

There were 300 target genes of miR-138 predicted by TargetScan.⁵⁴ Gene expression data (“cel” files of Affymetrix Human Genome U133 Plus 2.0 microarrays) of four $\gamma\delta$ T cells (GEO: GSE27291) and 14 HNSCC cells (GEO: GSE84557) were downloaded from the GEO database. The gene expression profiles were processed by R package “affy.” Data normalization was performed using “RMA” method. “PMA” callings for probes were also detected. Probes characterized with “Present” at a frequency of <50% in both cell types were filtered, resulting in 217 miR-138 targeted genes. Differential expression of miR-138 targeted genes in $\gamma\delta$ T cells and HNSCC cells was detected by t test. Multiple testing was adjusted by the Benjamini and Hochberg's FDR methods.⁵⁵ Genes with fold change ≥ 2 and

FDR < 0.01 were considered as differentially expressed between the two cell types. The biological and functional annotations of the differentially expressed genes were analyzed by the online tool DAVID.⁵⁶

Statistics

The comparisons of means among groups were analyzed by one-way ANOVA. All statistical analyses were performed using the SPSS package (version 13.0; SPSS, Chicago, IL, USA). A p value < 0.05 was considered statistically significant.

SUPPLEMENTAL INFORMATION

Supplemental Information includes two figures and can be found with this article online at <https://doi.org/10.1016/j.omtn.2018.11.009>.

AUTHOR CONTRIBUTIONS

Conception and Design: G.Z. and J.L.; Acquisition of Data: L.L., S.L., B.C., H.L., S.W., and S.H.; Analysis and Interpretation of Data: X.L. and J.J.; Writing and Review of the Manuscript: G.Z. and J.L.; Administrative, Technical, or Material Support: J.L.

CONFLICTS OF INTEREST

The authors declare no competing interests.

ACKNOWLEDGMENTS

This work was supported by the Department of Science and Technology of Sichuan Province (grants 2018JY0646, 2015SZ0053, and 2017JQ0040) and the National Natural Science Foundation of China (grants 81772900, 81672690, and 81872196).

REFERENCES

- Warnakulasuriya, S. (2009). Global epidemiology of oral and oropharyngeal cancer. *Oral Oncol.* 45, 309–316.
- Desiderio, V., Papagerakis, P., Tirino, V., Zheng, L., Matossian, M., Prince, M.E., Paino, F., Mele, L., Papaccio, F., Montella, R., et al. (2015). Increased fucosylation has a pivotal role in invasive and metastatic properties of head and neck cancer stem cells. *Oncotarget* 6, 71–84.
- Economopoulou, P., Agelaki, S., Perisanidis, C., Giotakis, E.I., and Psyrri, A. (2016). The promise of immunotherapy in head and neck squamous cell carcinoma. *Ann. Oncol.* 27, 1675–1685.
- Wu, D., Wu, P., Wu, X., Ye, J., Wang, Z., Zhao, S., Ni, C., Hu, G., Xu, J., Han, Y., et al. (2015). *Ex vivo* expanded human circulating V δ 1 $\gamma\delta$ T cells exhibit favorable therapeutic potential for colon cancer. *OncoImmunology* 4, e992749.
- Kondo, M., Sakuta, K., Noguchi, A., Ariyoshi, N., Sato, K., Sato, S., Sato, K., Hosoi, A., Nakajima, J., Yoshida, Y., et al. (2008). Zoledronate facilitates large-scale *ex vivo* expansion of functional gammadelta T cells from cancer patients for use in adoptive immunotherapy. *Cytotherapy* 10, 842–856.
- Silva-Santos, B., Serre, K., and Norell, H. (2015). $\gamma\delta$ T cells in cancer. *Nat. Rev. Immunol.* 15, 683–691.
- Brandes, M., Willmann, K., and Moser, B. (2005). Professional antigen-presentation function by human gammadelta T cells. *Science* 309, 264–268.
- Lo Presti, E., Dieli, F., and Meraviglia, S. (2014). Tumor-infiltrating $\gamma\delta$ T lymphocytes: pathogenic role, clinical significance, and differential programming in the tumor microenvironment. *Front. Immunol.* 5, 607.
- Rei, M., Pennington, D.J., and Silva-Santos, B. (2015). The emerging protumor role of $\gamma\delta$ T lymphocytes: implications for cancer immunotherapy. *Cancer Res.* 75, 798–802.

10. Menard, J.A., Cerezo-Magaña, M., and Belting, M. (2018). Functional role of extracellular vesicles and lipoproteins in the tumour microenvironment. *Philos. Trans. R. Soc. Lond. B Biol. Sci.* 373, 20160480.
11. Peinado, H., Lavotshkin, S., and Lyden, D. (2011). The secreted factors responsible for pre-metastatic niche formation: old sayings and new thoughts. *Semin. Cancer Biol.* 21, 139–146.
12. O’Loughlin, A.J., Woffindale, C.A., and Wood, M.J. (2012). Exosomes and the emerging field of exosome-based gene therapy. *Curr. Gene Ther.* 12, 262–274.
13. Mathivanan, S., Ji, H., and Simpson, R.J. (2010). Exosomes: extracellular organelles important in intercellular communication. *J. Proteomics* 73, 1907–1920.
14. Martins, V.R., Dias, M.S., and Hainaut, P. (2013). Tumor-cell-derived microvesicles as carriers of molecular information in cancer. *Curr. Opin. Oncol.* 25, 66–75.
15. Vader, P., Mol, E.A., Pasterkamp, G., and Schiffelers, R.M. (2016). Extracellular vesicles for drug delivery. *Adv. Drug Deliv. Rev.* 106 (Pt A), 148–156.
16. Zhang, D., Lee, H., Wang, X., Rai, A., Groot, M., and Jin, Y. (2018). Exosome-mediated small RNA delivery: a novel therapeutic approach for inflammatory lung responses. *Mol. Ther* 26, 2119–2130.
17. Ventimiglia, L.N., and Alonso, M.A. (2016). Biogenesis and function of T cell-derived exosomes. *Front. Cell Dev. Biol.* 4, 84.
18. Pitt, J.M., André, F., Amigorena, S., Soria, J.C., Eggermont, A., Kroemer, G., and Zitvogel, L. (2016). Dendritic cell-derived exosomes for cancer therapy. *J. Clin. Invest.* 126, 1224–1232.
19. Fais, S. (2013). NK cell-released exosomes: natural nanobullets against tumors. *OncoImmunology* 2, e22337.
20. Yoshikawa, T., Takahara, M., Tomiyama, M., Nieda, M., Maekawa, R., and Nakatsura, T. (2014). Large-scale expansion of $\gamma\delta$ T cells and peptide-specific cytotoxic T cells using zoledronate for adoptive immunotherapy. *Int. J. Oncol.* 45, 1847–1856.
21. Jin, Y., Chen, D., Cabay, R.J., Wang, A., Crowe, D.L., and Zhou, X. (2013). Role of microRNA-138 as a potential tumor suppressor in head and neck squamous cell carcinoma. *Int. Rev. Cell Mol. Biol.* 303, 357–385.
22. Wei, J., Nduom, E.K., Kong, L.Y., Hashimoto, Y., Xu, S., Gabrusiewicz, K., Ling, X., Huang, N., Qiao, W., Zhou, S., et al. (2016). miR-138 exerts anti-glioma efficacy by targeting immune checkpoints. *Neuro-oncol.* 18, 639–648.
23. Altvater, B., Pscherer, S., Landmeier, S., Kailayangiri, S., Savoldo, B., Juergens, H., and Rossig, C. (2012). Activated human $\gamma\delta$ T cells induce peptide-specific CD8⁺ T-cell responses to tumor-associated self-antigens. *Cancer Immunol. Immunother.* 61, 385–396.
24. Vantourout, P., and Hayday, A. (2013). Six-of-the-best: unique contributions of $\gamma\delta$ T cells to immunology. *Nat. Rev. Immunol.* 13, 88–100.
25. Lo Presti, E., Pizzolato, G., Gulotta, E., Cocorullo, G., Gulotta, G., Dieli, F., and Meraviglia, S. (2017). Current advances in $\gamma\delta$ T cell-based tumor immunotherapy. *Front. Immunol.* 8, 1401.
26. Tominaga, N., Yoshioka, Y., and Ochiya, T. (2015). A novel platform for cancer therapy using extracellular vesicles. *Adv. Drug Deliv. Rev.* 95, 50–55.
27. Zhu, L., Kalimuthu, S., Gangadaran, P., Oh, J.M., Lee, H.W., Baek, S.H., Jeong, S.Y., Lee, S.W., Lee, J., and Ahn, B.C. (2017). Exosomes derived from natural killer cells exert therapeutic effect in melanoma. *Theranostics* 7, 2732–2745.
28. Blanchard, N., Lankar, D., Faure, F., Regnault, A., Dumont, C., Raposo, G., and Hivroz, C. (2002). TCR activation of human T cells induces the production of exosomes bearing the TCR/CD3/zeta complex. *J. Immunol.* 168, 3235–3241.
29. Zitvogel, L., Regnault, A., Lozier, A., Wolfers, J., Flament, C., Tenza, D., Ricciardi-Castagnoli, P., Raposo, G., and Amigorena, S. (1998). Eradication of established murine tumors using a novel cell-free vaccine: dendritic cell-derived exosomes. *Nat. Med.* 4, 594–600.
30. Syn, N.L., Wang, L., Chow, E.K., Lim, C.T., and Goh, B.C. (2017). Exosomes in cancer nanomedicine and immunotherapy: prospects and challenges. *Trends Biotechnol.* 35, 665–676.
31. Kim, S.M., Yang, Y., Oh, S.J., Hong, Y., Seo, M., and Jang, M. (2017). Cancer-derived exosomes as a delivery platform of CRISPR/Cas9 confer cancer cell tropism-dependent targeting. *J. Control Release* 266, 8–16.
32. Bliss, S.A., Sinha, G., Sandiford, O.A., Williams, L.M., Engelberth, D.J., Guiro, K., Isenalmumbe, L.L., Greco, S.J., Ayer, S., Bryan, M., et al. (2016). Mesenchymal stem cell-derived exosomes stimulate cycling quiescence and early breast cancer dormancy in bone marrow. *Cancer Res.* 76, 5832–5844.
33. Kim, M.S., Haney, M.J., Zhao, Y., Yuan, D., Deygen, I., Klyachko, N.L., Kabanov, A.V., and Batrakova, E.V. (2018). Engineering macrophage-derived exosomes for targeted paclitaxel delivery to pulmonary metastases: in vitro and in vivo evaluations. *Nanomedicine (Lond.)* 14, 195–204.
34. Usman, W.M., Pham, T.C., Kwok, Y.Y., Vu, L.T., Ma, V., Peng, B., Chan, Y.S., Wei, L., Chin, S.M., Azad, A., et al. (2018). Efficient RNA drug delivery using red blood cell extracellular vesicles. *Nat. Commun.* 9, 2359.
35. Escudier, B., Dorval, T., Chaput, N., André, F., Caby, M.P., Novault, S., Flament, C., Lebloulaire, C., Borg, C., Amigorena, S., et al. (2005). Vaccination of metastatic melanoma patients with autologous dendritic cell (DC) derived-exosomes: results of the first phase I clinical trial. *J. Transl. Med.* 3, 10.
36. Besse, B., Charrier, M., Lapierre, V., Dansin, E., Lantz, O., Planchard, D., Le Chevalier, T., Livartoski, A., Barlesi, F., Laplanche, A., et al. (2015). Dendritic cell-derived exosomes as maintenance immunotherapy after first line chemotherapy in NSCLC. *OncoImmunology* 5, e1071008.
37. Moore, C., Kosgodage, U., Lange, S., and Inal, J.M. (2017). The emerging role of exosome and microvesicle- (EMV-) based cancer therapeutics and immunotherapy. *Int. J. Cancer* 141, 428–436.
38. Katakowski, M., Buller, B., Zheng, X., Lu, Y., Rogers, T., Osobamiro, O., Shu, W., Jiang, F., and Chopp, M. (2013). Exosomes from marrow stromal cells expressing miR-146b inhibit glioma growth. *Cancer Lett.* 335, 201–204.
39. Zhu, W., Huang, L., Li, Y., Zhang, X., Gu, J., Yan, Y., Xu, X., Wang, M., Qian, H., and Xu, W. (2012). Exosomes derived from human bone marrow mesenchymal stem cells promote tumor growth in vivo. *Cancer Lett.* 315, 28–37.
40. Lugini, L., Cecchetti, S., Huber, V., Luciani, F., Macchia, G., Spadaro, F., Paris, L., Abalsamo, L., Colone, M., Molinari, A., et al. (2012). Immune surveillance properties of human NK cell-derived exosomes. *J. Immunol.* 189, 2833–2842.
41. Kibria, G., Ramos, E.K., Wan, Y., Gius, D.R., and Liu, H. (2018). Exosomes as a drug delivery system in cancer therapy: potential and challenges. *Mol. Pharm.* 15, 3625–3633.
42. Muller, L., Simms, P., Hong, C.S., Nishimura, M.I., Jackson, E.K., Watkins, S.C., and Whiteside, T.L. (2017). Human tumor-derived exosomes (TEX) regulate Treg functions via cell surface signaling rather than uptake mechanisms. *OncoImmunology* 6, e1261243.
43. Tang, X.J., Sun, X.Y., Huang, K.M., Zhang, L., Yang, Z.S., Zou, D.D., Wang, B., Warnock, G.L., Dai, L.J., and Luo, J. (2015). Therapeutic potential of CAR-T cell-derived exosomes: a cell-free modality for targeted cancer therapy. *Oncotarget* 6, 44179–44190.
44. Kamekar, S., LeBleu, V.S., Sugimoto, H., Yang, S., Ruivo, C.F., Melo, S.A., Lee, J.J., and Kalluri, R. (2017). Exosomes facilitate therapeutic targeting of oncogenic KRAS in pancreatic cancer. *Nature* 546, 498–503.
45. Wong, T.S., Liu, X.B., Wong, B.Y., Ng, R.W., Yuen, A.P., and Wei, W.I. (2008). Mature miR-184 as potential oncogenic microRNA of squamous cell carcinoma of tongue. *Clin. Cancer Res.* 14, 2588–2592.
46. Liu, X., Chen, Z., Yu, J., Xia, J., and Zhou, X. (2009). MicroRNA profiling and head and neck cancer. *Comp. Funct. Genomics* 2009, 837514.
47. Manikandan, M., Deva Magendhra Rao, A.K., Rajkumar, K.S., Rajaraman, R., and Munirajan, A.K. (2015). Altered levels of miR-21, miR-125b-2*, miR-138, miR-155, miR-184, and miR-205 in oral squamous cell carcinoma and association with clinicopathological characteristics. *J. Oral Pathol. Med* 44, 792–800.
48. Sha, H.H., Wang, D.D., Chen, D., Liu, S.W., Wang, Z., Yan, D.L., Dong, S.C., and Feng, J.F. (2017). miR-138: A promising therapeutic target for cancer. *Tumour Biol.* 39, 1010428317697575.
49. Fu, D., Yu, W., Li, M., Wang, H., Liu, D., Song, X., Li, Z., and Tian, Z. (2015). MicroRNA-138 regulates the balance of Th1/Th2 via targeting RUNX3 in psoriasis. *Immunol. Lett.* 166, 55–62.

50. Kondo, M., Izumi, T., Fujieda, N., Kondo, A., Morishita, T., Matsushita, H., and Kakimi, K. (2011). Expansion of human peripheral blood $\gamma\delta$ T cells using zoledronate. *J. Vis. Exp.* 55, 3182.
51. Li, L., Li, C., Wang, S., Wang, Z., Jiang, J., Wang, W., Li, X., Chen, J., Liu, K., Li, C., and Zhu, G. (2016). Exosomes derived from hypoxic oral squamous cell carcinoma cells deliver miR-21 to normoxic cells to elicit a prometastatic phenotype. *Cancer Res.* 76, 1770–1780.
52. Roccaro, A.M., Sacco, A., Maiso, P., Azab, A.K., Tai, Y.T., Reagan, M., Azab, F., Flores, L.M., Campigotto, F., Weller, E., et al. (2013). BM mesenchymal stromal cell-derived exosomes facilitate multiple myeloma progression. *J. Clin. Invest.* 123, 1542–1555.
53. Bolstad, A.I., Eiken, H.G., Rosenlund, B., Alarcón-Riquelme, M.E., and Jonsson, R. (2003). Increased salivary gland tissue expression of Fas, Fas ligand, cytotoxic T lymphocyte-associated antigen 4, and programmed cell death 1 in primary Sjögren's syndrome. *Arthritis Rheum.* 48, 174–185.
54. Lewis, B.P., Burge, C.B., and Bartel, D.P. (2005). Conserved seed pairing, often flanked by adenosines, indicates that thousands of human genes are microRNA targets. *Cell* 120, 15–20.
55. Benjamini, Y., and Hochberg, Y. (1995). Controlling the false discovery rate: a practical and powerful approach to multiple testing. *J. R. Stat. Soc. Series B Stat. Methodol* 57, 289–300.
56. Huang da, W., Sherman, B.T., and Lempicki, R.A. (2009). Systematic and integrative analysis of large gene lists using DAVID bioinformatics resources. *Nat. Protoc.* 4, 44–57.